Delft University of Technology

Spatial noise correlations in a Si/SiGe two-qubit device from Bell state coherences

Boter, Jelmer M.; Xue, Xiao; Krähenmann, Tobias; Watson, Thomas F.; Premakumar, Vickram N.; Ward, Daniel R.; Savage, Donald E.; Eriksson, Mark A.; Vandersypen, Lieven M.K.; More Authors

Important note
To cite this publication, please use the final published version (if applicable).
Please check the document version above.

Spatial noise correlations in a Si/SiGe two-qubit device from Bell state coherences

Jelmer M. Boter [ORCID],[1] Xiao Xue [ORCID],[1] Tobias Krähenmann [ORCID],[1] Thomas F. Watson,[1] Vickram N. Premakumar,[2] Daniel R. Ward [ORCID],[2] Donald E. Savage,[2] Max G. Lagally,[2] Mark Friesen [ORCID],[2] Susan N. Coppersmith [ORCID],[2,*] Mark A. Eriksson,[2] Robert Joynt,[2] and Lieven M. K. Vandersypen [ORCID][1,3,†]

[1]*QuTech and Kavli Institute of Nanoscience, Delft University of Technology, Lorentzweg 1, 2628 CJ Delft, The Netherlands*
[2]*University of Wisconsin-Madison, Madison, Wisconsin 53706, USA*
[3]*Components Research, Intel Corporation, 2501 NE Century Blvd, Hillsboro, Oregon 97124, USA*

We study spatial noise correlations in a Si/SiGe two-qubit device with integrated micromagnets. Our method relies on the concept of decoherence-free subspaces, whereby we measure the coherence time for two different Bell states, designed to be sensitive only to either correlated or anticorrelated noise, respectively. From these measurements we find weak correlations in low-frequency noise acting on the two qubits, while no correlations could be detected in high-frequency noise. We expect nuclear spin noise to have an uncorrelated nature. A theoretical model and numerical simulations give further insight into the additive effect of multiple independent (anti)correlated noise sources with an asymmetric effect on the two qubits as can result from charge noise. Such a scenario in combination with nuclear spins is plausible given the data and the known decoherence mechanisms. This work is highly relevant for the design of optimized quantum error correction codes for spin qubits in quantum dot arrays, as well as for optimizing the design of future quantum dot arrays.

Large-scale quantum computers will need to rely on quantum error correction (QEC) to deal with the inevitable qubit errors caused by interaction with the environment and by imperfect control signals. The noise amplitude can vary from qubit to qubit and furthermore can exhibit correlations or anticorrelations between qubits. Most QEC error thresholds, such as the 1% threshold for the surface code [1], are derived under the assumption of negligible correlations in qubit errors. Other approaches, such as decoherence-free subspaces (DFSs) [2], are designed under the assumption of correlated noise, taking advantage of symmetry considerations to reduce the qubit sensitivity to external noise. Examples for quantum dot based qubits include the singlet-triplet qubit [3,4] and the quadrupole qubit [5]. In addition, QEC schemes exist that can deal with short-range correlations in the noise [6]. Spatial noise correlations have therefore been studied extensively, both theoretically [7–14] and experimentally [11,15,16].

Semiconductor quantum dots are promising hosts for spin qubits in quantum computation [17], because of their favorable scaling and excellent coherence properties. Silicon, in particular, has excellent properties for long-lived spin qubits: intrinsic spin-orbit coupling is weak and hyperfine interaction is small [18]. The hyperfine interaction can even be reduced further by isotopic purification. In addition, silicon quantum dot fabrication is largely compatible with conventional CMOS industry, which allows large-scale manufacturing of silicon

spin qubits and on-chip integration of classical control electronics [19]. In recent years, significant progress has been made with silicon spin qubits, showing tens of milliseconds coherence times [20], high-fidelity single- [20–22] and two-qubit gates [23,24], quantum algorithms [25], strong spin-photon coupling [26,27], and long-distance spin-spin coupling [28].

The most important decoherence sources in natural silicon quantum dots are the hyperfine interaction with nuclear spins and charge noise. Nuclear spin noise is typically uncorrelated between adjacent dots [29]. Charge noise is usually caused by distant fluctuating charges [30–32], which is expected to lead to spatial correlations on the length scale of interdot distances of 100 nm or less. In the presence of a magnetic field gradient, which is commonly used for qubit selectivity and fast qubit control, qubits are sensitive to electric field fluctuations and charge noise will impact spin coherence [21,33]. However, a quantitative measurement of spatial noise correlations in an actual two-qubit device is lacking.

Here we study experimentally spatial noise correlations in a Si/SiGe two-qubit device, by preparing Bell states in either the parallel or the antiparallel subspace, similarly to recent work with NV centers in diamond [34]. Via a Ramsey-style experiment, we find that Bell states in the antiparallel subspace show a ~30% longer dephasing time than those in the parallel subspace. A Hahn-echo style measurement reveals no detectable difference in the decay time for the respective Bell states. We present a simple model to describe noise correlations on two qubits, including asymmetric noise amplitudes acting on the two qubits, and study numerically the combined effect of multiple (anti)correlated, asymmetric noise sources. We use these simulations to assess which combinations of

———
*Present address: School of Physics, University of New South Wales, Sydney NSW 2052, Australia.
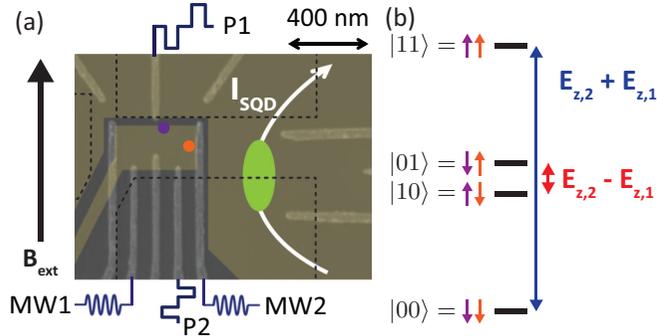†Corresponding author: l.m.k.vandersypen@tudelft.nl

FIG. 1. (a) Scanning electron micrograph of a similar Si/SiGe device as used in the measurements, showing the depletion gates used to define the potential landscape in the 2D electron gas accumulated by the yellow shaded gates (drawn digitally). Purple and orange circles indicate the estimated positions of the two dots, occupied by one electron each, and the ellipse indicates a sensing quantum dot. Two-qubit operations are controlled via gate voltage pulses applied to gates P1 and P2, and microwave signals for single-qubit control are applied to gates MW1 and MW2. The contours of cobalt micromagnets are indicated by the dashed black lines. (b) Energy level diagram for two qubits in an inhomogeneous magnetic field, giving rise to a difference in Zeeman energy between the two qubits.

FIG. 2. $T_{2,|\Psi\rangle}^*$ extracted from Eq. (1): (a) as a function of correlation factor ρ and noise amplitude $\sigma_1 = \sigma_2$, and (b) as a function of σ_1 and σ_2 for $\rho = 1$. Insets show the corresponding images for $T_{2,|\Phi\rangle}^*$. Contours correspond to (0.5, 0.75, 1.0, 1.25, 1.5, 1.75) μs. In all images an uncorrelated noise contribution corresponding to a Bell state coherence time of 2.0 μs is added to prevent singularities.

noise sources are compatible with the observed coherence times.

Figure 1(a) shows a schematic of the device used in this work, which is the same as described earlier [23,25]. It comprises an electrostatically defined double quantum dot (DQD) in a two-dimensional electron gas (2DEG). The 2DEG is confined in a 12-nm-thick silicon quantum well, 37 nm below the surface of an undoped Si/SiGe heterostructure with natural isotope composition. On top of the heterostructure, we fabricate two gate layers with cobalt micromagnets. The device is cooled down to $T \approx 30$ mK and subject to an external magnetic field of $B_{\text{ext}} = 617$ mT. Suitable voltages are applied to accumulation and fine gates (in the top and bottom layer, respectively) to form a DQD in the single-electron regime. Single-electron spin states are Zeeman split by the total magnetic field, and used to encode two single-spin qubits. The micromagnets ensure individual qubit addressability by a gradient in the longitudinal magnetic field, resulting in spin resonance frequencies of 18.35 and 19.61 GHz for qubit 1 (Q1) and qubit 2 (Q2), respectively.

Figure 1(b) shows the resulting energy level diagram for the two qubits. For perfectly correlated noise, fluctuations in the Zeeman energy for both qubits are the same: $\delta E_{Z,1} = \delta E_{Z,2} = \delta E_Z$. Consequently, the sum of the two qubit energies fluctuates, $\Delta(E_{Z,1} + E_{Z,2}) = 2\delta E_Z$, while their difference is not affected, $\Delta(E_{Z,1} - E_{Z,2}) = 0$. On the other hand, for perfectly anticorrelated noise $\delta E_{Z,1} = -\delta E_{Z,2}$, and the opposite holds for the sum and difference energies. Bell states consist of superpositions of the two-spin eigenstates and allow us to study dephasing between these eigenstates. An antiparallel Bell state, which evolves in time at a rate proportional to the difference of the single-qubit energies, will be affected by anticorrelated noise, but not by correlated noise. A parallel Bell state, which evolves in time at a rate proportional to
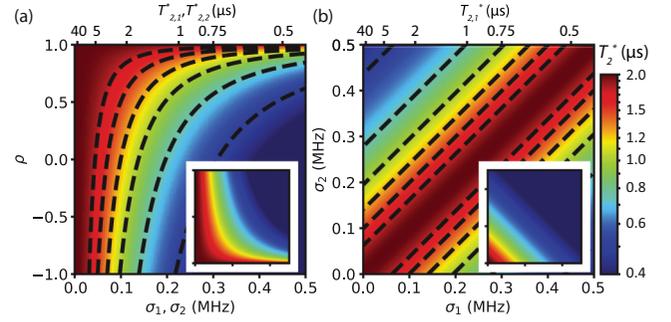
the sum of the single-qubit energies, is sensitive to correlated noise, but not to anticorrelated noise. Such properties are exploited in DFSs and are used here as a probe for spatial correlations in the noise acting on the qubits.

Real systems are often subject to both uncorrelated and (anti)correlated noise. Furthermore, the noise amplitudes acting on different qubits are generally different, regardless of whether the noise is uncorrelated or (anti)correlated. We wish to capture all these scenarios in one unified theoretical formalism. We include pure dephasing only, which is justified by the long T_1 times for spin qubits compared to the experiment and coherence timescales, and assume a quasistatic Gaussian joint probability distribution for the noise acting on the two qubits. We can then express the two-qubit coherence times for an antiparallel $[|\Psi\rangle = (|\downarrow\uparrow\rangle - i|\uparrow\downarrow\rangle)/\sqrt{2}]$ and a parallel $[|\Phi\rangle = (|\downarrow\downarrow\rangle - i|\uparrow\uparrow\rangle)/\sqrt{2}]$ Bell state quantitatively as follows (see the Supplemental Material [35]):

$$\left(\frac{1}{T_{2,|\Psi\rangle}^*}\right)^2 = 2\pi^2\left(\sigma_1^2 + \sigma_2^2 - 2\rho\sigma_1\sigma_2\right),$$
$$\left(\frac{1}{T_{2,|\Phi\rangle}^*}\right)^2 = 2\pi^2\left(\sigma_1^2 + \sigma_2^2 + 2\rho\sigma_1\sigma_2\right),$$

(1)

where σ_i^2 is the variance of the noise in the resonance frequency of qubit i [the single-qubit coherence time is given by $(\frac{1}{T_{2,i}^*})^2 = 2\pi^2\sigma_i^2$], and ρ is a correlation factor ($-1 \leqslant \rho \leqslant 1$). Positive ρ indicates correlations, while negative ρ indicates anticorrelations.

The effect of the noise amplitudes σ_i and the correlation factor ρ on the coherence time for the antiparallel Bell state $T_{2,|\Psi\rangle}^*$ is visualized in Fig. 2(a). Here $\sigma_1 = \sigma_2$, so for $\rho = 1$, $|\Psi\rangle$ forms a true DFS and the noise has no effect regardless of its amplitude. With decreasing ρ, $T_{2,|\Psi\rangle}^*$ decreases, as the noise becomes initially less correlated ($\rho > 0$), then uncorrelated ($\rho = 0$) and eventually anticorrelated ($\rho < 0$). For $\rho = -1$, $T_{2,|\Psi\rangle}^*$ is only one fourth of the single-qubit coherence times. For $T_{2,|\Phi\rangle}^*$, the corresponding image is mirrored around $\rho = 0$, see the inset of Fig. 2(a), and the longest coherence time occurs for $\rho = -1$. Figure 2(b) shows the effect of

asymmetric noise amplitudes on the two qubits for $\rho = 1$. We see that despite the maximal correlation factor, a true DFS only exists for symmetric noise ($\sigma_1 = \sigma_2$) and $|\Psi\rangle$ decoheres when $\sigma_1 \neq \sigma_2$. Clearly both the correlation factor and the asymmetry in the noise impact the two-qubit coherence.

From Eq. (1) we see that, as anticipated, experimental measurement of the decay times for the parallel and antiparallel Bell states reveals whether (anti)correlations in the noise acting on the two qubits are present. In order to quantify the correlation factor ρ, measurements of the single-qubit decay times are needed as well. We now summarize the experimental procedure; for more information on the measurement setup and individual qubit characteristics, see the Supplemental Material [35] and Ref. [25]. Q2 is initialized and read out via spin-selective tunneling to a reservoir [36]. Initialization of Q1 to its ground state is done by fast spin relaxation at a hotspot [37], and readout of Q1 is performed by mapping its spin state onto Q2 via a controlled-rotation (CROT) gate followed by spin readout of Q2 [25]. For single-qubit driving we exploit an artificial spin-orbit coupling, induced by cobalt micromagnets, for electric dipole spin resonance (EDSR) [38]. The two-qubit gate relies on the exchange interaction between the two qubits, controlled by gate voltage pulses. We operate in the regime where the Zeeman energy difference between the two qubits exceeds the two-qubit exchange interaction strength, hence the native two-qubit gate is the controlled-phase gate [25,39,40].

Concretely, we perform two-qubit measurements analogous to the measurement of Ramsey fringes to measure the decay of Bell state coherences over time [13]. As shown in the circuits in Figs. 3(a) and 3(c), we prepare $|\Psi\rangle$ or $|\Phi\rangle$ and after a varying free evolution time we reverse the sequence to ideally return to the $|00\rangle$ state. In every run of the experiment, we measure both spins in single-shot mode and determine the two-spin probabilities from repeated experiment runs. The two-spin probabilities are normalized and a Gaussian decay is fit to the $|00\rangle$ return probability. To improve the fit of the decay, we add an evolution-time dependent phase to the first microwave pulse applied to Q2 after the delay time [see $Z(\Delta\varphi)$ in Figs. 3(a) and 3(c)], so that the measured $|00\rangle$ probability oscillates. We first test the measurement procedure via artificially introduced dephasing from random rotations of each spin around its quantization axis, implemented in software via Pauli frame updates. The decay observed for the antiparallel (parallel) Bell state is independent of the noise amplitude when the same (opposite) random rotations are applied to both spins, but increases when opposite (the same) random rotations are applied to the two spins, as expected. This validates the measurement protocol.

Figures 3(b) and 3(d) show typical decay curves for $|\Psi\rangle$ and $|\Phi\rangle$, respectively, when subject to natural noise only. A scatter plot of repeated measurements, Fig. 3(e), shows a systematically longer T_2^* for $|\Psi\rangle$ than for $|\Phi\rangle$, indicating correlations in the noise. Using Eq. (1), derived for quasistatic noise, we can extract from the decay of $|\Psi\rangle$ and $|\Phi\rangle$ a lower bound for the correlation factor $\rho \geqslant 0.27 \pm 0.02$ (see the Supplemental Material [35]). In order to go beyond a lower bound and determine an estimate of ρ from Eq. (1), we also need at least one of the single-qubit dephasing times, which we measured to be $T_{2,1}^* = 0.97 \pm 0.02\ \mu s$ and $T_{2,2}^* = 0.59 \pm 0.02\ \mu s$.
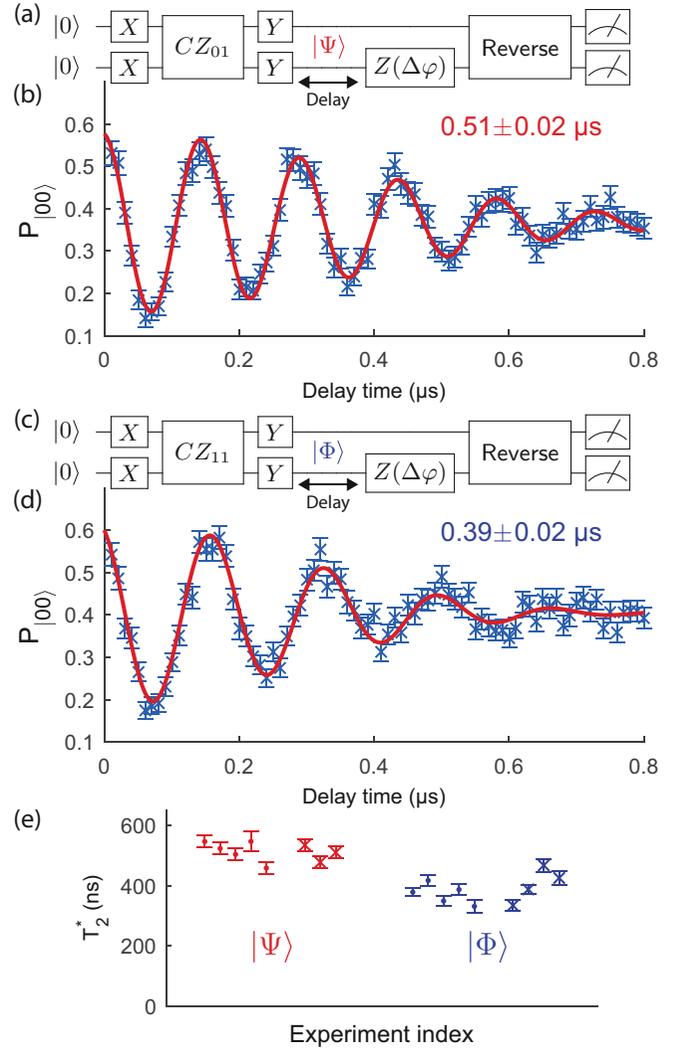

FIG. 3. (a) and (c) Circuit diagrams for two-qubit experiments analogous to the measurement of Ramsey fringes. The gate sequences are designed such that single-qubit rotations are always applied simultaneously to both qubits, avoiding idle times that would lead to faster dephasing. Here $CZ_{ij}|m, n\rangle = (-1)^{\delta(i,m)\delta(j,n)}|m, n\rangle$ for $i, j, m, n \in \{0, 1\}$ are the primitive two-qubit gates, constructed from a CZ gate with duration $t = \pi\hbar/J$ and single-qubit rotations [25]. (b) and (d) Typical $|00\rangle$ return probability as a function of delay time for (b) $|\Psi\rangle$ and (d) $|\Phi\rangle$. The data are fit with a sinusoidal function with Gaussian decay, $P_{|00\rangle} \propto e^{-(t/T_2^*)^2}$. Error bars are based on a Monte Carlo method by assuming a multinomial distribution for the measured two-spin probabilities and are $\pm 1\sigma$ from the mean [25]. We attribute the slight difference in oscillation frequency between (b) and (d) to crosstalk effects during frequency calibration, as for example observed in Refs. [23,25,41]. (e) Scatter plot of decay times for $|\Psi\rangle$ and $|\Phi\rangle$ for two measurement runs separated by $\sim$50 h (points and crosses). Every data point is averaged over $\sim$100 min. The average coherence times are 513 ± 8 and 387 ± 6 ns for $|\Psi\rangle$ and $|\Phi\rangle$, respectively. Error bars are $\pm 1\sigma$ from the mean.

Using both single-qubit T_2^*s in Eq. (1) gives an overdetermined system of equations. We proceed by keeping $T_{2,1}^*/T_{2,2}^*$ equal to the measured ratio, and obtain a modest correlation factor, $\rho = 0.31 \pm 0.03$ (see the Supplemental Material [35]).
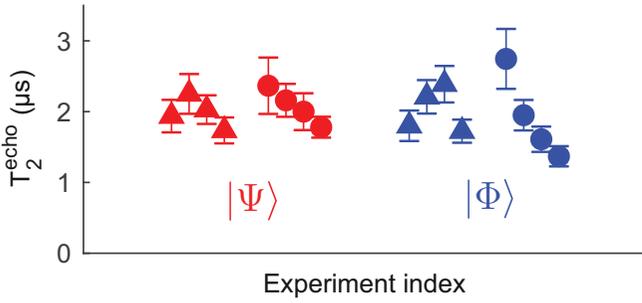
FIG. 4. Scatter plot of the two-qubit coherence times obtained in Hahn-echo style measurements for $|\Psi\rangle$ and $|\Phi\rangle$, from a fit to the data with an exponentially decaying sinusoidal function ($P_{|00\rangle} \propto e^{-t/T_2^*}$). Triangles represent data points where the Hahn echo pulses applied to both qubits are rotations around the $\hat{x}$ axis. For the circles, the rotation of Q1 is around $\hat{x}$ and the rotation of Q2 is around $\hat{y}$. Data points are averaged over $\sim$[47, 66, 100, 148] min. The average two-qubit Hahn echo coherence times are 2.03 ± 0.09 and 1.98 ± 0.09 μs for $|\Psi\rangle$ and $|\Phi\rangle$, respectively. Error bars are $\pm 1\sigma$ from the mean.

We note that in keeping $T_{2,1}^*/T_{2,2}^*$ fixed, Eq. (1) returns a value for σ_1 and σ_2 that is $\sim$15% larger than the measured value. The discrepancy may be in part due to the fact that the simple model that leads to Eq. (1) assumes quasistatic Gaussian noise. This is a commonly made assumption in simple models of silicon spin qubits, but various experiments showed higher-frequency noise to be relevant as well [20,22,25]. However, a more detailed model that accounts for non-quasistatic noise is beyond the scope of this work.

In order to gain insight into the frequency dependence of the spatial noise correlations, we perform measurements analogous to Hahn echo measurements. Here the delay times seen in the circuit diagrams of Figs. 3(a) and 3(c) contain 180 deg rotations around the $\hat{x}$ or $\hat{y}$ axis applied to the two qubits, which reverse the time evolution resulting from static noise contributions (see the Supplemental Material [35] for circuit diagrams and details). The results are presented in Fig. 4. The echo pulses prolong the two-qubit coherence times by a factor of $\sim$4–5. We do not, however, observe a systematic difference in the echo decay times for the parallel versus antiparallel Bell states, meaning there are no detectable spatial correlations in higher-frequency noise, and the correlations found in the Ramsey-style measurements of Fig. 3 are mostly present in the low-frequency part of the spectrum. The data presented in Figs. 3 and 4 form a complete data set with repeated measurements, all performed with very similar gate voltage settings.

We observe only modest correlations in the noise. In this natural silicon substrate the hyperfine interaction with ^{29}Si nuclear spins, for which little or no spatial correlations are expected [29], is likely to contribute significantly. In the Supplemental Material [35] we estimate the separate contributions to the noise and we estimate the correlation factor in the charge noise only to be $\rho = 0.5$–0.6. In order to more reliably assess the spatial noise correlations arising from charge noise only, it would be helpful to repeat the experiments presented here in an isotopically purified ^{28}Si sample.

In addition to noise that is uncorrelated by itself, multiple noise sources that produce correlated noise on the qubits can add up to give rise to noise that is mostly uncorrelated as well. This can be seen from the following observations. Multiple independently fluctuating noise sources each producing perfectly correlated noise ($\rho = 1$) with the same relative amplitude on the two qubits, are equivalent to a single (stronger) source of perfectly correlated noise with this same relative amplitude on the two qubits. However, randomly distributed relative amplitudes with random sign would rapidly render the combined noise indistinguishable from uncorrelated noise.

Different relative amplitudes can occur for charge noise from multiple charge fluctuators close to the dots, which couple to the spin states through the magnetic field gradient. Also remote charge fluctuators can give rise to different noise amplitudes on the two spins, for instance when the tightness of the confining potential, the local magnetic field gradient or the gate screening differs between the dots (indeed Table S3 reveals that Q2 is much more sensitive to electric fields than Q1 [35]). In the Supplemental Material [35] we illustrate this effect with an example simulation and describe it mathematically.

Based on this discussion, a picture emerges where the combination of noise from multiple distant charge fluctuators, which affect the qubits asymmetrically due to their different confining potentials and nuclear spin noise, is responsible for the (weak) spatial noise correlations at low frequency.

In summary, we have demonstrated a method to quantitatively study spatial noise correlations based on the coherence of Bell states in a Si/SiGe two-qubit device. Experimentally we observe small spatial correlations in low-frequency noise, while for higher-frequency noise correlations appear to be absent. Applying this method to an isotopically purified silicon spin qubit device will yield more quantitative information on correlations present in charge noise only. Our findings on the importance of asymmetric coupling of noise sources to two (or more) qubits can be exploited for reducing or enhancing spatial correlations in the noise in any qubit platform. For the case of spin qubits in quantum dots, this can be done for instance through a device design with engineered differences in confining potential or magnetic field gradient. In this respect, qubits encoded in two-electron spin states in dot-donor systems offer an extreme difference in confining potential [42]. We anticipate that the optimization of future quantum error correction codes will go hand in hand with the design of qubits that either maximize or minimize spatial noise correlations, as has been done in for example Ref. [43].

Data supporting the findings of this study are available online [44].

[1] D. S. Wang, A. G. Fowler, and L. C. L. Hollenberg, Phys. Rev. A **83**, 020302(R) (2011).

[2] D. A. Lidar, I. L. Chuang, and K. B. Whaley, Phys. Rev. Lett. **81**, 2594 (1998).

[3] J. Levy, Phys. Rev. Lett. **89**, 147902 (2002).

[4] J. R. Petta, A. C. Johnson, J. M. Taylor, E. A. Laird, A. Yacoby, M. D. Lukin, C. M. Marcus, M. P. Hanson, and A. C. Gossard, Science **309**, 2180 (2005).

[5] M. Friesen, J. Ghosh, M. A. Eriksson, and S. N. Coppersmith, Nat. Commun. **8**, 15923 (2017).

[6] J. Preskill, arXiv:1207.6131.

[7] Á. Rivas and M. Müller, New J. Phys. **17**, 062001 (2015).

[8] P. Szańkowski, M. Trippenbach, and Ł. Cywiński, Phys. Rev. A **94**, 012109 (2016).

[9] G. A. Paz-Silva, L. M. Norris, and L. Viola, Phys. Rev. A **95**, 022121 (2017).

[10] J. Krzywda, P. Szańkowski, J. Chwedeńczuk, and Ł. Cywiński, Phys. Rev. A **98**, 022329 (2018).

[11] L. Postler, Á. Rivas, P. Schindler, A. Erhard, R. Stricker, D. Nigg, T. Monz, R. Blatt, and M. Müller, Quantum **2**, 90 (2018).

[12] D. Kwiatkowski and Ł. Cywiński, Phys. Rev. B **98**, 155202 (2018).

[13] V. N. Premakumar and R. Joynt, arXiv:1812.07076.

[14] J. Krzywda, P. Szańkowski, and Ł. Cywiński, New J. Phys. **21**, 043034 (2019).

[15] T. Monz, P. Schindler, J. T. Barreiro, M. Chwalla, D. Nigg, W. A. Coish, M. Harlander, W. Hänsel, M. Hennrich, and R. Blatt, Phys. Rev. Lett. **106**, 130506 (2011).

[16] A. Ozaeta and P. L. McMahon, Quantum Sci. Technol. **4**, 025015 (2019).

[17] D. Loss and D. P. DiVincenzo, Phys. Rev. A **57**, 120 (1998).

[18] F. A. Zwanenburg, A. S. Dzurak, A. Morello, M. Y. Simmons, L. C. L. Hollenberg, G. Klimeck, S. Rogge, S. N. Coppersmith, and M. A. Eriksson, Rev. Mod. Phys. **85**, 961 (2013).

[19] L. M. K. Vandersypen, H. Bluhm, J. S. Clarke, A. S. Dzurak, R. Ishihara, A. Morello, D. J. Reilly, L. R. Schreiber, and M. Veldhorst, npj Quantum Inf. **3**, 34 (2017).

[20] M. Veldhorst, J. C. C. Hwang, C. H. Yang, A. W. Leenstra, B. de Ronde, J. P. Dehollain, J. T. Muhonen, F. E. Hudson, K. M. Itoh, A. Morello, and A. S. Dzurak, Nat. Nanotechnol. **9**, 981 (2014).

[21] E. Kawakami, T. Jullien, P. Scarlino, D. R. Ward, D. E. Savage, M. G. Lagally, V. V. Dobrovitski, M. Friesen, S. N. Coppersmith, M. A. Eriksson, and L. M. K. Vandersypen, Proc. Natl. Acad. Sci. **113**, 11738 (2016).

[22] J. Yoneda, K. Takeda, T. Otsuka, T. Nakajima, M. R. Delbecq, G. Allison, T. Honda, T. Kodera, S. Oda, Y. Hoshi, N. Usami, K. M. Itoh, and S. Tarucha, Nat. Nanotechnol. **13**, 102 (2018).

[23] X. Xue, T. F. Watson, J. Helsen, D. R. Ward, D. E. Savage, M. G. Lagally, S. N. Coppersmith, M. A. Eriksson, S.

Wehner, and L. M. K. Vandersypen, Phys. Rev. X **9**, 021011 (2019).

[24] W. Huang, C. H. Yang, K. W. Chan, T. Tanttu, B. Hensen, R. C. C. Leon, M. A. Fogarty, J. C. C. Hwang, F. E. Hudson, K. M. Itoh, A. Morello, A. Laucht, and A. S. Dzurak, Nature (London) **569**, 532 (2019).

[25] T. F. Watson, S. G. J. Philips, E. Kawakami, D. R. Ward, P. Scarlino, M. Veldhorst, D. E. Savage, M. G. Lagally, M. Friesen, S. N. Coppersmith, M. A. Eriksson, and L. M. K. Vandersypen, Nature (London) **555**, 633 (2018).

[26] N. Samkharadze, G. Zheng, N. Kalhor, D. Brousse, A. Sammak, U. C. Mendes, A. Blais, G. Scappucci, and L. M. K. Vandersypen, Science **359**, 1123 (2018).

[27] X. Mi, M. Benito, S. Putz, D. M. Zajac, J. M. Taylor, G. Burkard, and J. R. Petta, Nature (London) **555**, 599 (2018).

[28] F. Borjans, X. G. Croot, X. Mi, M. J. Gullans, and J. R. Petta, Nature (London) **577**, 195 (2020).

[29] E. A. Chekhovich, M. N. Makhonin, A. I. Tartakovskii, A. Yacoby, H. Bluhm, K. C. Nowack, and L. M. K. Vandersypen, Nat. Mater. **12**, 494 (2013).

[30] S. W. Jung, T. Fujisawa, Y. Hirayama, and Y. H. Jeong, Appl. Phys. Lett. **85**, 768 (2004).

[31] E. Paladino, Y. M. Galperin, G. Falci, and B. L. Altshuler, Rev. Mod. Phys. **86**, 361 (2014).

[32] F. Beaudoin and W. A. Coish, Phys. Rev. B **91**, 165432 (2015).

[33] A. Kha, R. Joynt, and D. Culcer, Appl. Phys. Lett. **107**, 172101 (2015).

[34] C. E. Bradley, J. Randall, M. H. Abobeih, R. C. Berrevoets, M. J. Degen, M. A. Bakker, M. Markham, D. J. Twitchen, and T. H. Taminiau, Phys. Rev. X **9**, 031045 (2019).

[35] See Supplemental Material at http://link.aps.org/supplemental/10.1103/PhysRevB.101.235133, including additional Refs. [45,46], for more details on the noise model, experimental details, method validation, quantification of the observed correlations, notes on the effect of nuclear spin noise and the Bell state fidelity, echo experiments, simulation results, and the effect of adding multiple noise sources.

[36] J. M. Elzerman, R. Hanson, L. H. Willems van Beveren, B. Witkamp, L. M. K. Vandersypen, and L. P. Kouwenhoven, Nature (London) **430**, 431 (2004).

[37] V. Srinivasa, K. C. Nowack, M. Shafiei, L. M. K. Vandersypen, and J. M. Taylor, Phys. Rev. Lett. **110**, 196803 (2013).

[38] M. Pioro-Ladrière, Y. Tokura, T. Obata, T. Kubo, and S. Tarucha, Appl. Phys. Lett. **90**, 024105 (2007).

[39] T. Meunier, V. E. Calado, and L. M. K. Vandersypen, Phys. Rev. B **83**, 121403(R) (2011).

[40] M. Veldhorst, C. H. Yang, J. C. C. Hwang, W. Huang, J. P. Dehollain, J. T. Muhonen, S. Simmons, A. Laucht, F. E.

Hudson, K. M. Itoh, A. Morello, and A. S. Dzurak, Nature (London) **526**, 410 (2015).

[41] K. Takeda, J. Yoneda, T. Otsuka, T. Nakajima, M. R. Delbecq, G. Allison, Y. Hoshi, N. Usami, K. M. Itoh, S. Oda, T. Kodera, and S. Tarucha, npj Quantum Inf. **4**, 54 (2018).

[42] P. Harvey-Collard, N. T. Jacobson, M. Rudolph, J. Dominguez, G. A. Ten Eyck, J. R. Wendt, T. Pluym, J. K. Gamble, M. P. Lilly, M. Pioro-Ladrière, and M. S. Carroll, Nat. Commun. **8**, 1029 (2017).

[43] D. Layden, M. Chen, and P. Cappellaro, Phys. Rev. Lett. **124**, 020504 (2020).

[44] J. M. Boter, X. Xue, T. Krähenmann, T. F. Watson, V. N. Premakumar, D. R. Ward, D. E. Savage, M. G. Lagally, M. Friesen, S. N. Coppersmith, M. A. Eriksson, R. Joynt, and L. M. K. Vandersypen, Zenodo (2020).

[45] L. M. K. Vandersypen and I. L. Chuang, Rev. Mod. Phys. **76**, 1037 (2005).

[46] J. T. Muhonen, J. P. Dehollain, A. Laucht, F. E. Hudson, R. Kalra, T. Sekiguchi, K. M. Itoh, D. N. Jamieson, J. C. McCallum, A. S. Dzurak, and A. Morello, Nat. Nanotechnol. **9**, 986 (2014).